ORIGINAL ARTICLE

Comparison of Myocardial Ischemia Detection Between Semiconductor and Conventional Anger-type Three-detector SPECT

Hiroto Yoneyama, PhD[1)], Kenichi Nakajima, MD[2)], Junichi Taki, MD[3)], Hiroshi Wakabayashi, MD[3)], Takahiro Konishi, RT[1)], Takayuki Shibutani, PhD[4)], Koichi Okuda, PhD[5)] and Masahisa Onoguchi, PhD[4)]

Received: April 2, 2021/Revised manuscript received: July 5, 2021/Accepted: August 2, 2021

Abstract

***Objective*: Although semiconductor single-photon emission computed tomography (D-SPECT) has been used for myocardial perfusion imaging, few studies have compared its ability to detect myocardial ischemia with that of 3-detector SPECT (GCA9300R). This study used invasive coronary angiography to determine whether the detectability of myocardial ischemia differs between D-SPECT and GCA9300R.**

***Materials and methods*: This study included 24 patients who were assessed by coronary angiography within 60 days of myocardial perfusion D-SPECT and GCA9300R. Two nuclear medicine physicians interpreted myocardial perfusion D-SPECT and GCA9300R images with five grades of confidence, then defined regions of ischemia on polar maps. The gold standard was determined by another nuclear cardiology specialist based on integrated assessment of the coronary angiography findings and other clinical information derived from medical charts. The concordance rate and the Cohen kappa (κ) between D-SPECT and GCA9300R were calculated.**

***Results*: The sensitivity, specificity, negative and positive predictive values, and the accuracy of patient-based diagnoses were 66.7%, 91.7%, 89.2%, 72.8%, and 85.5%, respectively, for GCA9300R, and 83.3%, 83.3%, 93.7%, 62.4%, and 83.3%, respectively, for D-SPECT. Interpretations of ischemia did not uncover any significant differences between D-SPECT and GCA9300R. The Cohen κ values of D-SPECT and GCA9300 agreed substantially, moderately and marginally for the left circumflex coronary artery (LCX) (0.68), right coronary artery (RCA) (0.43), and left anterior descending coronary artery (LAD) (0.39), respectively.**

***Conclusions*: The detectability of myocardial ischemia is comparable between D-SPECT and GCA9300R. Sensitivity is better for D-SPECT than GCA9300R. However, false-positive D-SPECT findings, especially in the apex and inferior wall should be interpreted with caution.**

Keywords: Cadmium zinc telluride semiconductor, Coronary artery disease, Myocardial perfusion imaging, Nuclear cardiology, D-SPECT

Ann Nucl Cardiol 2021; 7 (1): 49–56

Six decades have passed since Anger developed a means of detecting gamma-rays using sodium iodide (NaI) crystals and a photomultiplier tube, which is now called an Anger-type scintillation camera (1). More recent single-photon emission computed tomography (SPECT) systems using cadmium zinc telluride (CZT) semiconductor detectors have become popular for cardiac studies (2–3). The count sensitivity is 10-fold higher for D-SPECT than conventional Anger-type 2-detector SPECT systems (2). Although the performance of semiconductor SPECT systems (D-SPECT; Spectrum Dynamics Medical, Inc., Sarasota, FL, USA) has been investigated in detail (4–6), few studies have compared it

doi: 10.17996/anc.21-00141

1) Department of Radiological Technology, Kanazawa University Hospital, Ishikawa, Japan
2) Department of Functional Imaging and Artificial Intelligence, Kanazawa University, Ishikawa, Japan
3) Department of Biotracer Medicine, Graduate School of Medical Science, Kanazawa University, Ishikawa, Japan
4) Department of Health Science, Graduate School of Medical Science, Kanazawa University, Ishikawa, Japan
5) Department of Physics, Kanazawa Medical University, Ishikawa, Japan

Table 1 Patient demographics

Items	Mean ± SD, N (%)
Number	24
Age (y)	73.3 ± 8.6 (58–87)
Sex (male/female)	20 (83.3%)/4 (16.7%)
Body mass index (kg/m^2)	22.8 ± 2.9 (18.6–27.6)
Body height (cm)	162 ± 10.2 (140–177.5)
Body weight (kg)	60.0 ± 11.6 (38.5–85.9)
^{99m}Tc-Sestamibi/tetrofosmin	11 (45.8%)/13 (54.2%)
eGFR (mL/min/1.73 m^2)	57.1 ± 24.5 (4.5–88.7)
Hypertension	21 (87.5%)
Diabetes mellitus	16 (66.7%)
Dyslipidemia	14 (58.3%)
Obesity (BMI ≥25 kg/m^2)	5 (20.8%)
Chronic kidney failure (eGFR <15 mL/min/1.73 m^2)	2 (8.3%)
History of PCI	6 (20.8%)
History of CABG	3 (12.5%)
Angiographic findings	
No significant stenosis	9 (37.5%)
Number of coronary artery stenosis	
1 Vessel disease	7 (29.2%)
2 Vessel disease	5 (20.8%)
3 Vessel disease	3 (12.5%)
Regions of vessels with ≥50% stenosis	
LAD	8 (33.3%)
LCX	9 (37.5%)
RCA	9 (37.5%)
Regions of vessels with ≥75% stenosis	
LAD	6 (25.0%)
LCX	7 (29.2%)
RCA	7 (29.2%)

BMI: body mass index, CABG: coronary artery bypass grafting, CKF: chronic kidney failure, eGFR: estimated glomerular filtration rate, LAD: left anterior descending coronary artery, LCX: left circumflex coronary artery, PCI: percutaneous coronary intervention, RCA: right coronary artery, SD: standard deviation.

with conventional Anger-type 3-detector SPECT (GCA 9300R; Canon Medical Systems Corp., Otawara City, Japan). The triple-headed, GCA9300R SPECT consists of gamma cameras forming a triangular aperture in a rotating gantry, which provides one of the best myocardial image among Anger-type cameras qualities at present. It has 1.5-fold better count sensitivity than conventional 2-detector SPECT (7). In contrast, D-SPECT can acquire images more rapidly (3–8 min), but might be subject to artefactual decreases occurring in the inferior wall slightly below the apex (8). Thus, the present study aimed to determine whether detectability differs between myocardial ischemia using high-performance cameras of D-SPECT and GCA9300R within the same group of patients using visual analyses.

Materials and methods

Table 1 shows the characteristics of the patients. The study group comprised 24 patients who were assessed by myocardial perfusion SPECT using D-SPECT and GCA9300R on the same day, and by coronary angiography (CAG) within 60 days thereafter. All patients underwent stress myocardial perfusion imaging (MPI) using a one-day stress-rest protocol with adenosine infused at 120 μg/kg/min for 6 min. Either 250–370 MBq of ^{99m}Tc-sestamibi (MIBI; FUJIFILM Toyama Chemical Co. Ltd., Tokyo, Japan) or tetrofosmin (Nihon Medi-Physics Co. Ltd., Tokyo, Japan) was injected 3 min after starting the adenosine infusion, then 740 MBq of ^{99m}Tc-tetrofosmin or MIBI was administered to the patients at rest. Data were acquired using the two SPECT systems — 60 min after the

injection. All cases were initially evaluated with GCA9300R and then with D-SPECT. Approval for retrospective, observational study was obtained from the institution's ethical committee.

Three-detector SPECT (GCA9300R)

The GCA9300R (Canon, Tokyo, Japan) consisted of triple-headed gamma cameras in a 120° configuration equipped with a low-energy, high-resolution (LEHR) collimator. The parameters were as follows: 128×128 matrix, zoom 1.0, 3.2 mm pixels, and 60s per projection, acquisition duration 20 min. We obtained 60 frames, at 6° intervals over 360°. The energy was centered at 140.5 keV with a 20% window. Scatter and attenuation were not corrected. The detectors were placed close to the patient in a circular orbit with a radius of 20–23 cm. Data were reconstructed using a three-dimensional iterative method based on an ordered subset expectation maximization (3D-OSEM) algorithm with resolution recovery and 100 updates (10 subsets × 10 iterations). The ordered subset expectation maximization (OSEM) algorithm included an 8th order Butterworth filter with a cutoff of 0.45 cycles/cm.

Semiconductor SPECT (D-SPECT)

The D-SPECT (Spectrum Dynamics Medical Japan, Tokyo, Japan) consisted of nine detectors arranged around the myocardium and a wide-angle, parallel-hole tungsten collimator. The SPECT data were acquired using the following parameters: 64×64 matrix, zoom 1.0, 4.92 mm pixel, 120 views/detector, 1.5 M counts, and acquisition periods of 5–8 and 2–3 min for stress and rest studies, respectively. Energy was centered at 140.5 keV with a 20 % window. Scatter and attenuation were not corrected. Data were reconstructed using a Spectrum Dynamics (SD) and OSEM algorithm with resolution recovery and 224 updates (32 subsets × 7 iterations).

Interpretation of images

The gold standard of ischemia was determined by a nuclear cardiology specialist with >40 years of experience, all available clinical information. Since patients with old myocardial infarction, percutaneous coronary intervention (PCI), and coronary artery bypass grafting (CABG) were included, the final diagnosis could not simply be defined based on the degree of coronary stenosis or fractional flow reserve (FFR). Therefore, the gold standard was determined using CAG, FFR and clinical information comprising myocardial perfusion SPECT data, coronary computed tomographic angiography (CCTA) data, the medical history of patients, and the subsequent clinical course. Significant coronary artery disease was defined as stenosis in at least one coronary artery, indicated by FFR 0.80 or less, or ischemia using myocardial perfusion SPECT if the FFR was missing. The nuclear medicine physicians A and B, with 38 and 14 years of experience with nuclear cardiology, respectively, initially evaluated the D-SPECT images, then the GCA9300R images four weeks later. The grades of confidence (1–5) used to evaluate their interpretation of regional abnormalities were definitely normal, probably normal, equivocal, probably abnormal, and definitely abnormal, respectively. The grade ≥4 was defined as abnormal.

Statistical analysis

All data were statistically analyzed using EZR (Saitama Medical Center, Jichi Medical University, Saitama, Japan), a graphical user interface for R 2.13.0 (R Foundation for Statistical Computing, Vienna, Austria) (9). We evaluated the detectability of ischemia based on areas under receiver operating characteristics (ROC) curves (AUC). The concordance rate and the Cohen κ between D-SPECT and GCA9300R were calculated. All statistical tests were two-tailed, and values with $p<0.05$ were considered statistically significant.

Results

The concordance rate and Cohen κ

The concordance rate and Cohen κ of D-SPECT and GCA9300 are 87.5% and 0.43 for the right coronary artery (RCA), 87.5% and 0.39 for the left anterior descending coronary artery (LAD), 94.8% and 0.68 for the left circumflex coronary artery (LCX), respectively. The concordance rate and Cohen κ of D-SPECT and GCA9300 are 83.3% and 0.24 for the anterior wall, 81.2% and 0.20 for the apex, 81.2% and 0.20 for the inferior wall, 91.7% and 0.55 for the septal wall, 93.8% and 0.54 for the lateral wall, respectively. The findings of ischemia differed between D-SPECT and GCA9300R in the apex and inferior wall.

Patient-based diagnosis of myocardial ischemia

The AUC of patient-based diagnosis using GCA9300R and D-SPECT did not significantly differ (Figure 1). The sensitivity, specificity, negative (NPV) and positive (PPV) predictive values, and the accuracy of patient-based diagnoses were 66.7%, 91.7%, 89.2%, 72.8%, and 85.5%, respectively, for GCA9300R, and 83.3%, 83.3%, 93.7%, 62.4%, and 83.3%, respectively, for D-SPECT with SD-reconstruction algorithm. When OSEM-reconstruction algorithm was used, these values were 83.3%, 83.3%, 93.7%, 62.4%, and 83.3%, respectively, showing equivalent diagnostic accuracy (Figure 2).

Coronary artery-based diagnosis of myocardial ischemia

The AUC of coronary artery-based diagnosis using GCA 9300R and D-SPECT in RCA, LAD, and LCX did not

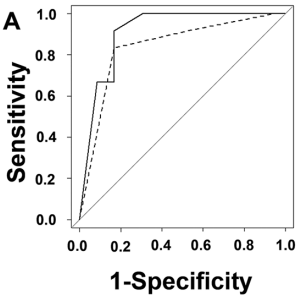

	Patient-based diagnosis AUC (95%CI)	Coronary artery-based diagnosis AUC (95%CI)		
		RCA	LAD	LCX
D-SPECT	0.840 (0.707-0.974)	0.826 (0.727-0.925)	0.771 (0.562-0.980)	0.946 (0.881-1.000)
GCA9300R	0.911 (0.834-0.988)	0.744 (0.563-0.925)	0.849 (0.663-1.000)	0.875 (0.707-1.000)
p - value	0.289	0.482	0.289	0.442

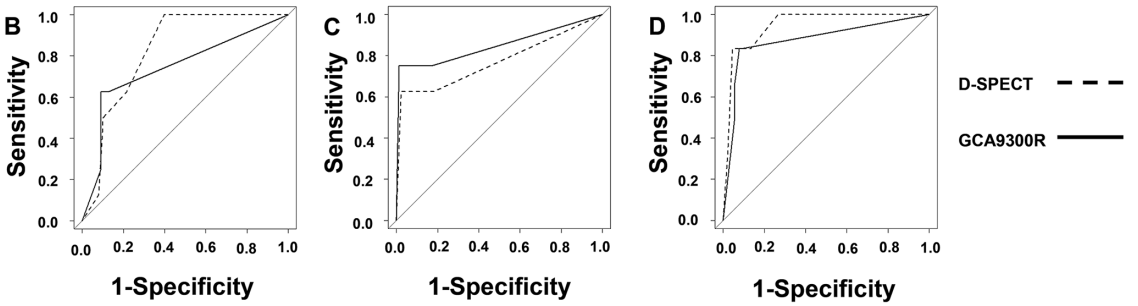

Figure 1　Detectability of myocardial ischemia, D-SPECT vs. GCA9300R.

Performance indicators of D-SPECT, and GCA9300R images to detect ischemia in patients based on visual evaluation (A). Ability of D-SPECT and GCA9300R imaging to detect ischemia in coronary arteries based on visual evaluation. Areas under receiver operating characteristics (ROC) curves derived from visual evaluation of RCA (B), LAD (C), and LCX (D) on D-SPECT and GCA9300R images. AUC derived from patient-based and coronary arteries based on visual evaluation.

AUC: areas under ROC curves, CI: confidence interval, LAD: left anterior descending coronary artery, LCX: left circumflex coronary artery, RCA: right coronary artery, ROC: receiver operating characteristics, SPECT: single-photon emission computed tomography.

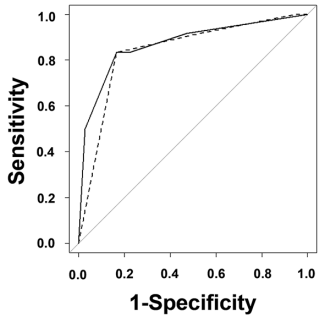

	Patient-based diagnosis AUC (95%CI)
D-SPECT (SD)	0.840 (0.707-0.974)
D-SPECT (OSEM)	0.870 (0.741-1.000)
p - value	0.303

D-SPECT (SD)

D-SPECT (OSEM)

Figure 2　Detectability of myocardial ischemia, SD vs. OSEM.

Areas under ROC curves derived from analysis of D-SPECT with SD-reconstruction algorithm and OSEM-reconstruction algorithm to detect ischemia in patients based on visual evaluation.

OSEM: ordered subset expectation maximization, ROC: receiver operating characteristics, SD: Spectrum Dynamics, SPECT: single-photon emission computed tomography.

significantly differ (Figure 1). The accuracy of coronary-based diagnoses in RCA, LAD, and LCX was 84.8%, 90.3%, and 94.1%, respectively, for D-SPECT and 84.2%, 94.1%, and 88.6%, respectively, for GCA9300R. Figure 3 shows that prominent extra-cardiac activity adjacent to an inferior wall defect on rest GCA9300R images obscured reversibility, whereas the count was marginally reduced in the inferoapical region on D-SPECT. As slight differences in extent of abnormality were found between GCA9300R and D-SPECT images, Figure 4 shows a patient with single-vessel (LCX) disease. Only slight ischemia was identified from the GCA9300R and D-SPECT images, which did not cause significant difference in clinical interpretation. Figure 5 shows a case with a discrepancy in the range and extent of ischemia between D-SPECT and GCA9300R.

Discussion

This is the first study to directly compare the abilities of two high performance cameras (D-SPECT, GCA9300R), and integrated invasive CAG to detect myocardial ischemia in a

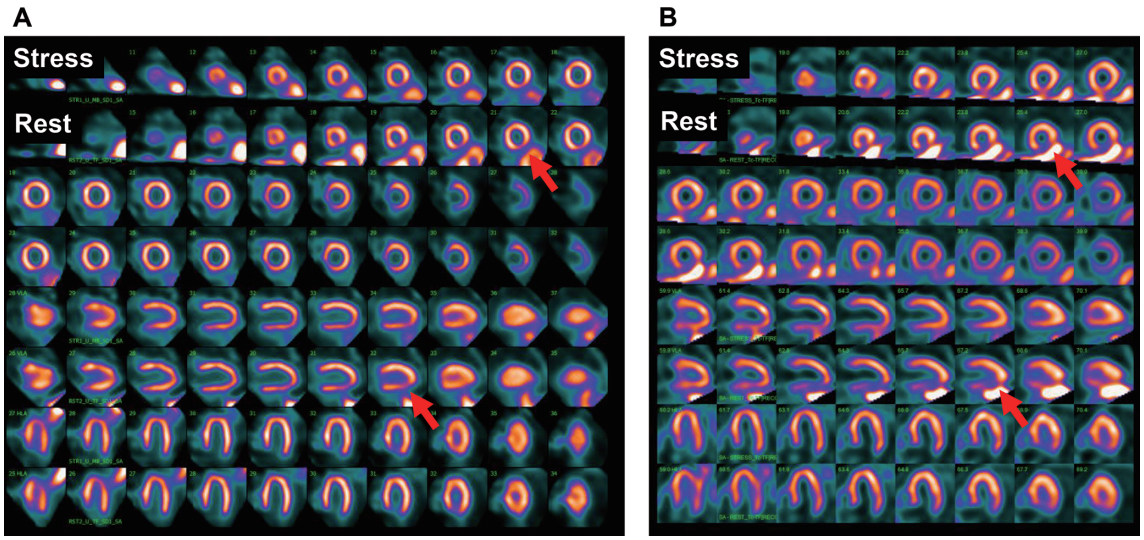

Figure 3 Short axis, vertical long axis, horizontal long axis images of D-SPECT and GCA9300R.
Artefacts due to extra-cardiac uptake (arrow) in D-SPECT (A) and GCA9300R (B). These artefacts were reduced using D-SPECT.
SPECT: single-photon emission computed tomography.

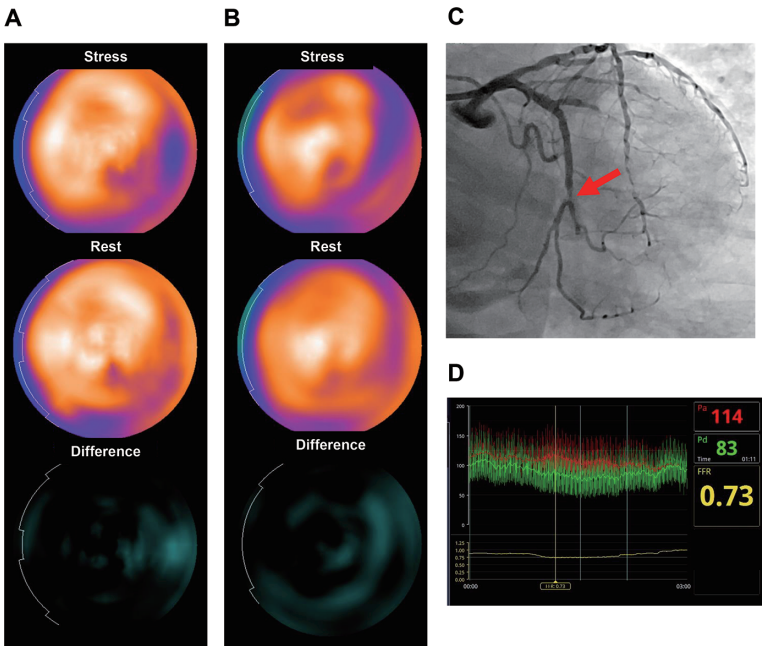

Figure 4 Typical ischemic findings of a 75-year-old man with angina pectoris.
(A) D-SPECT, (B) GCA9300R, and CAG, revealed 75% stenosis in LCX (C) (Arrow). Stress-induced ischemia and infarcts in lateral walls were diagnosed by consensus interpretation. Defect SSS, SRS, and SDS were respectively 13, 7, and 6 determined by D-SPECT, and 16, 11, 5, determined by GCA9300R. FFR is 0.73 (D).
CAG: coronary angiography, FFR: fractional flow reserve, LCX: left circumflex coronary artery, SDS: summed difference score, SPECT: single-photon emission computed tomography, SRS: summed rest score, SSS: summed stress score, SPECT: single-photon emission computed tomography.

single group of patients. The findings of visual evaluation showed that the detectability of myocardial ischemia using GCA9300R and D-SPECT did not significantly differ.

Advantage of D-SPECT over conventional camera

The sensitivity and energy resolution of D-SPECT with a CZT detector is superior to that of conventional SPECT with NaI (Tl) scintillation crystals (2), and it is more diagnostically accurate than the conventional Anger camera (4, 10).

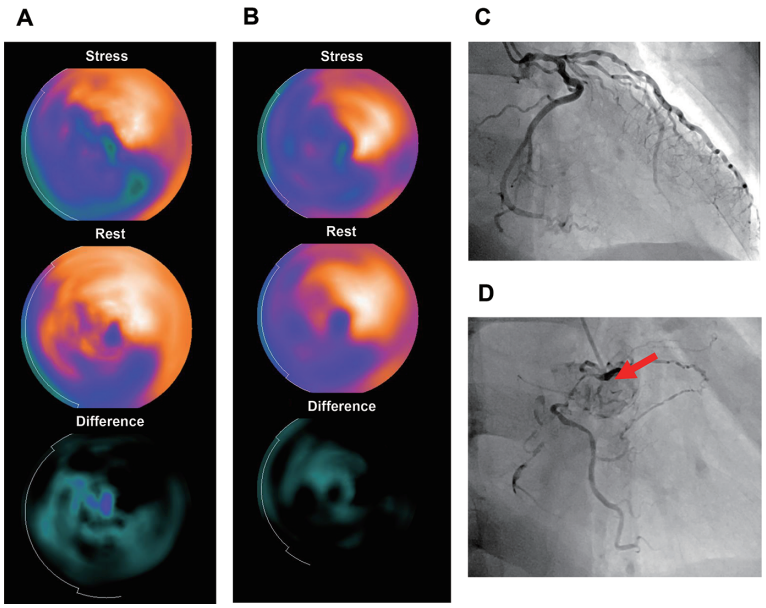

Figure 5 Typical ischemic findings of a 62-year-old man with angina pectoris.
(A) D-SPECT, (B) GCA9300R, and CAG revealed 50% stenosis in LMT, 90% stenosis in LAD #6, #7, #9, and 100% stenosis in LCX #12 (C). CAG revealed 100% stenosis in RCA (D) (Arrow). Stress-induced ischemia and infarcts in anterior, septal, apex, and inferior walls were diagnosed by consensus interpretation. Defect SSS, SRS, and SDS were respectively 26, 12, and 14 determined by D-SPECT, and 22, 13, 8, determined by GCA9300R.
CAG: coronary angiography, LAD: left anterior descending coronary artery, LCX: left circumflex coronary artery, LMT: left main coronary trunk, RCA: right coronary artery, SDS: summed difference score, SPECT: single-photon emission computed tomography, SRS: summed rest score, SSS: summed stress score.

Acquisition is generally more comfortable for patients, who are upright during D-SPECT imaging. In addition, artefacts potentially caused by extra-cardiac uptake in subdiaphragmatic organs while seated, were reduced by upright D-SPECT image acquisition.

Advantage of GCA9300R over conventional camera

Technical specification of the GCA9300R has been improved as follows. The conventional 2-detector SPECT mainly uses a 3 inch photomultiplier tube (PMT), while the GCA9300R uses a 2 inch PMT. Since the PMTs of GCA 9300R are arranged at a higher density (more than twice) compared with conventional 2-detector SPECT, locations of gamma rays can be detected accurately, which contributes to improved uniformity. The resolution correction compensates for the deterioration of the spatial resolution caused by the distance between the collimators and a patient (11, 12). In GCA9300R, the processing parameters of iterative method are also optimized so as to suppress the artifact due to Gibbs oscillation generated by the resolution correction.

Cautions regarding D-SPECT

Although the duration of image acquisition is significantly reduced by D-SPECT, artefacts should be avoided as much as possible. The quality of D-SPECT images can be reduced by movements of patients, incorrect positioning, breast attenuation, and obesity, all of which might decrease specificity (8). The findings of ischemia in the apex and inferior wall differed between D-SPECT and GCA9300R. The low apex and apical counts might have been be caused by anatomical thinning of the myocardium, which can be explained by a partial volume effect that is dependent on myocardial thickness (13). Since the detector is fixed in front of the chest for D-SPECT imaging, regional counts in the anterior and lateral walls are less attenuated, resulting in high spatial resolution and few artefacts. The pitfalls and artefacts of conventional gamma cameras, and methods of preventing and correcting them have been established (14). Patient motion is one of the most prevalent and important sources of artefacts in images acquired using Anger cameras and D-SPECT (8). Deep breathing and coughing can also create artefacts. However, although vertical or horizontal motion can be easily detected on sonograms, technologists should ensure that patients are comfortable before starting acquisition to minimize the likelihood of motion. Since the duration of D-SPECT imaging is relatively short, image acquisition can easily be repeated if motion influences the quality of perfusion data. The advanced SD reconstruction of D-SPECT images incorporating resolution recovery and heart-prior assumptions might not always be optimal in clinical situations such as hypertrophy and large

defects (15, 16). Since the appearance of wall thickness differs depending on the reconstruction method, secondary reconstruction by OSEM is recommended for D-SPECT when findings differ between reconstructed and other diagnostic images.

Accuracy of myocardial perfusion SPECT to detect coronary artery disease

A summary of 16 studies (n=2,092 patients) revealed that the diagnostic sensitivity and specificity of semiconductor SPECT were 84% [95% confidence interval (CI), 78%–89%] and 69% (95% CI, 62%–76%) respectively (4). A comparison of scatter segmentation and photo-peak window data (SSPAC) and non-correction methods for diagnosing individual coronary territories showed that the vessel-based diagnostic ability, sensitivity, specificity, and positive and negative predictive values of the 3-detector SPECT with and without attenuation correction using SSPAC were 77%, 89%, 74%, and 90%, and 51%, 87%, 62%, and 82%, respectively (17). Although diagnostic ability depends on patient selection criteria, the present findings between the modalities were comparable, which supported our conclusions.

Limitations

Several limitations of this single-center, retrospective, observational study of a small patient cohort should be considered. Various conditions of the patients could not be evaluated. The selection of data was biased by clinical conditions, such as coronary revascularization. Few of our patients were female or obese. Therefore, artefacts such as breast attenuation and obesity might have been avoided, which might have been a factor involved in the high diagnostic accuracy.

Conclusions

The ability of D-SPECT and three-headed GCA9300R to detect myocardial ischemia is comparable. However, counts were lower near the apex and inferior wall in D-SPECT images, indicating that evaluators should become thoroughly acquainted with the image characteristics of Anger and CZT, as well as Anger cameras.

Acknowledgments

The authors thank Norma Foster for editorial assistance. We are grateful to the nuclear medicine physicians at Kanazawa University Hospital who interpreted the myocardial perfusion images and provided clinical information. We are grateful to the radiology technologists at Kanazawa University Hospital for providing technical support.

Sources of finding

None.

Conflicts of interest

None.

Reprint requests and correspondence:
Hiroto Yoneyama, PhD
Department of Radiological Technology, Kanazawa University Hospital, 13-1 Takara-machi, Kanazawa 920-8641 Japan
E-mail: kizu@cf6.so-net.ne.jp

References

1. Anger HO. Scintillation camera with multichannel collimators. J Nucl Med 1964; 5: 515–31.
2. Gambhir SS, Berman DS, Ziffer J, et al. A novel high-sensitivity rapid-acquisition single-photon cardiac imaging camera. J Nucl Med 2009; 50: 635–43.
3. Johnson RD, Bath NK, Rinker J, et al. Introduction to the D-SPECT for Technologists: Workflow Using a Dedicated Digital Cardiac Camera. J Nucl Med Technol 2020; 48: 297–303.
4. Nudi F, Iskandrian AE, Schillaci O, Peruzzi M, Frati G, Biondi-Zoccai G. Diagnostic accuracy of myocardial perfusion imaging with CZT technology: systemic review and meta-analysis of comparison with invasive coronary angiography. JACC Cardiovasc Imaging 2017; 10: 787–94.
5. Takahasi Y, Miyagawa M, Nishiyama Y, Ishimura H, Mochizuki T. Performance of a semiconductor SPECT system: comparison with a conventional Anger-type SPECT instrument. Ann Nucl Med 2013; 27: 11–6.
6. Cantoni V, Green R, Acampa W, et al. Diagnostic performance of myocardial perfusion imaging with conventional and CZT single-photon emission computed tomography in detecting coronary artery disease: A meta-analysis. J Nucl Cardiol 2019; 28: 698–715.
7. Kouris K, Clarke GA, Jarritt PH, Townsend CE, Thomas SN. Physical performance evaluation of the Toshiba GCA-9300 A triple-headed system, J Nucl Med 1993; 34: 1778–89.
8. Allie R, Hutton BF, Prvulovich E, Bomanji J, Michopoulou S, Ben-Haim S. Pitfalls and artifacts using the D-SPECT dedicated cardiac camera. J Nucl Cardiol 2016; 23: 301–10.
9. Kanda Y. Investigation of the freely available easy-to-use software ‘EZR’ for medical statistics. Bone Marrow Transplant 2013; 48: 452–8.
10. Nakajima K, Matsuo S, Kawano M, et al. The validity of multi-center common normal database for identifying myocardial ischemia: Japanese Society of Nuclear Medicine working group database. Ann Nucl Med 2010; 24: 99–105.
11. Onishi H, Motomura N, Fujino K, Natsume T, Haramoto Y. Quantitative performance of advanced resolution recovery strategies on SPECT images: evaluation with use of digital phantom models. Radiol Phys Technol 2013; 6: 42–53.
12. Okuda K, Nakajima K, Yamada M, et al. Optimization of

iterative reconstruction parameters with attenuation correction, scatter correction and resolution recovery in myocardial perfusion SPECT/CT. Ann Nucl Med 2014; 28: 60–8.
13. Okuda K, Nakajima K, Matsuo S, Wakabayashi H, Taki J, Kinuya S. Cause of apical thinning on attenuation-corrected myocardial perfusion SPECT. Nucl Med Commun 2011; 32: 1033–9.
14. Burrell S, MacDonald A. Artifacts and pitfalls in myocardial perfusion imaging. J Nucl Med Technol 2006; 34: 193–211.
15. Tsuboi K, Nagaki A, Shibutani T, Onoguchi M. Optimal choice of OSEM and SD reconstruction algorithms in CZT SPECT for hypertrophic cardiomyopathy patients. J Nucl Cardiol 2019; 28: 236–44.
16. Nakajima K, Yoneyama H, Slomka P. Beware the pitfalls of beauty: High-quality myocardial images with resolution recovery. J Nucl Cardiol 2019; 26: 574–8.
17. Yamauchi Y, Kanzaki Y, Hayashi M, et al. Improved diagnosis of the number of stenosed coronary artery vessels by segmentation with scatter and photo-peak window data for attenuation correction in myocardial perfusion SPECT. J Nucl Cardiol 2019; 26: 574–81.